Estuarine, Coastal and Shelf Science 151 (2014) 169–180

Contents lists available at ScienceDirect

Estuarine, Coastal and Shelf Science

journal homepage: www.elsevier.com/locate/ecss

Seasonal variability of total suspended matter in Minas Basin, Bay of Fundy

Jing Tao [a, *], Paul S. Hill [a], Ryan P. Mulligan [b], Peter C. Smith [c]

[a] Department of Oceanography, Dalhousie University, Halifax, NS, B3H 4R2, Canada
[b] Department of Civil Engineering, Queen's University, Kingston, ON, K7L 3N6, Canada
[c] Fisheries and Oceans Canada, Bedford Institute of Oceanography, Dartmouth, NS, B2Y 4A2, Canada

A R T I C L E I N F O

Article history:
Received 17 April 2014
Accepted 8 October 2014
Available online 16 October 2014

Keywords:
Bay of Fundy
Minas Basin
ocean colour
total suspended matter
satellite observations
numerical modelling
sediment transport
seasonal variability

A B S T R A C T

Total suspended matter (TSM) concentrations were derived from ocean colour imagery (MERIS satellite data) in Minas Basin. Analysis of time series of TSM in 1-km^2 pixel boxes revealed an annual cycle in TSM in most parts of the Basin. Higher TSM of up to 85 g/m^3 was observed in late-winter (February–March), and lower TSM of 5–10 g/m^3 characterized late-summer (July–August). The largest annual variation occurred in the centre of Basin, and the smallest variation occurred in shallow areas. Satellite-derived TSM, supported by *in situ* observations, were compared to predictions using the Delft3D model. Increasing model erosion rate in winter relative to summer improved agreement between model and satellite-derived TSM. In comparison with the satellite-derived estimates, the model underestimated TSM in shallow areas in summer and overestimated it in winter. This discrepancy is likely due to inaccurate satellite-derived TSM in shallow, high-concentration areas of the Basin.

1. Introduction

Macrotidal estuaries are ecologically diverse and productive environments that are affected by anthropogenic processes (Bianchi, 2007). They are important centers of human population and shipping (Mitchell and Uncles, 2013), and they are also an attractive target for development of tidal power (Morris, 2013). These environments are characterized by tidal ranges greater than 4 m (see Hayes, 1975) and large total suspended matter (TSM) concentrations. The large TSM concentrations affect productivity, water quality, navigation, and coastal defence, so understanding of the factors that cause large TSM concentrations is vital to effective and sustainable use of these environments (Mitchell and Uncles, 2013; Morris, 2013). Tidal currents, waves, and sediment input from rivers all affect TSM in macrotidal estuaries, but biological processes may also play a significant role, primarily by binding bottom sediments with biofilms that make them less erodible (Mitchell and Uncles, 2013). The goal of this research is to investigate linkages between seasonal changes in TSM and seabed erodibility in Minas Basin of the Bay of Fundy in eastern Canada.

The Bay of Fundy is a large macrotidal embayment situated on the east coast of Canada between the provinces of New Brunswick and Nova Scotia. It is characterized by a semi-diurnal tidal regime with a maximum tidal range of 16.3 m and high suspended sediment concentrations (van Proosdij et al., 2009). The Minas Basin system extends off the central Bay of Fundy to the east, and it has been divided into four regions: Minas Channel, Minas Passage, Minas Basin and Cobequid Bay (Fig. 1a). The ocean environment in Minas Basin is dominated by wind, waves and tidal currents (Fader et al., 1977). The resident suspended sediment volume in Minas Basin was calculated to be 3×10^7 m^3 (Greenberg and Amos, 1983). The abundance of sediment in Minas Basin is the result of erosion of Triassic sandstone cliffs that surround the shoreline, supplemented by the input of glacial outwash sand and clay (Thomas, 1976; Stea, 2003). The area of the tidal flats in Minas Basin is about 358 km^2 in extent, almost half of it in Cobequid Bay. The TSM in Cobequid Bay is much higher than that in the Bay's tributary rivers where the tidal influence is weak. The high concentration of suspended sediment at the sea surface is likely related to the re-suspension of mud from intertidal mudflats through wave and current activity (Dalrymple et al., 1990).

The temporal-spatial distribution of TSM in the Bay of Fundy is complex (Dalrymple et al., 1990). Previously *in situ* sampling, remote sensing and numerical modelling have been used to understand sediment dynamics in the study area. *In situ* observations

* Corresponding author.
E-mail addresses: jing.tao@dal.ca (J. Tao), paul.hill@dal.ca (P.S. Hill), mulligar@queensu.ca (R.P. Mulligan), Peter.Smith@dfo-mpo.gc.ca (P.C. Smith).

http://dx.doi.org/10.1016/j.ecss.2014.10.005
0272-7714/

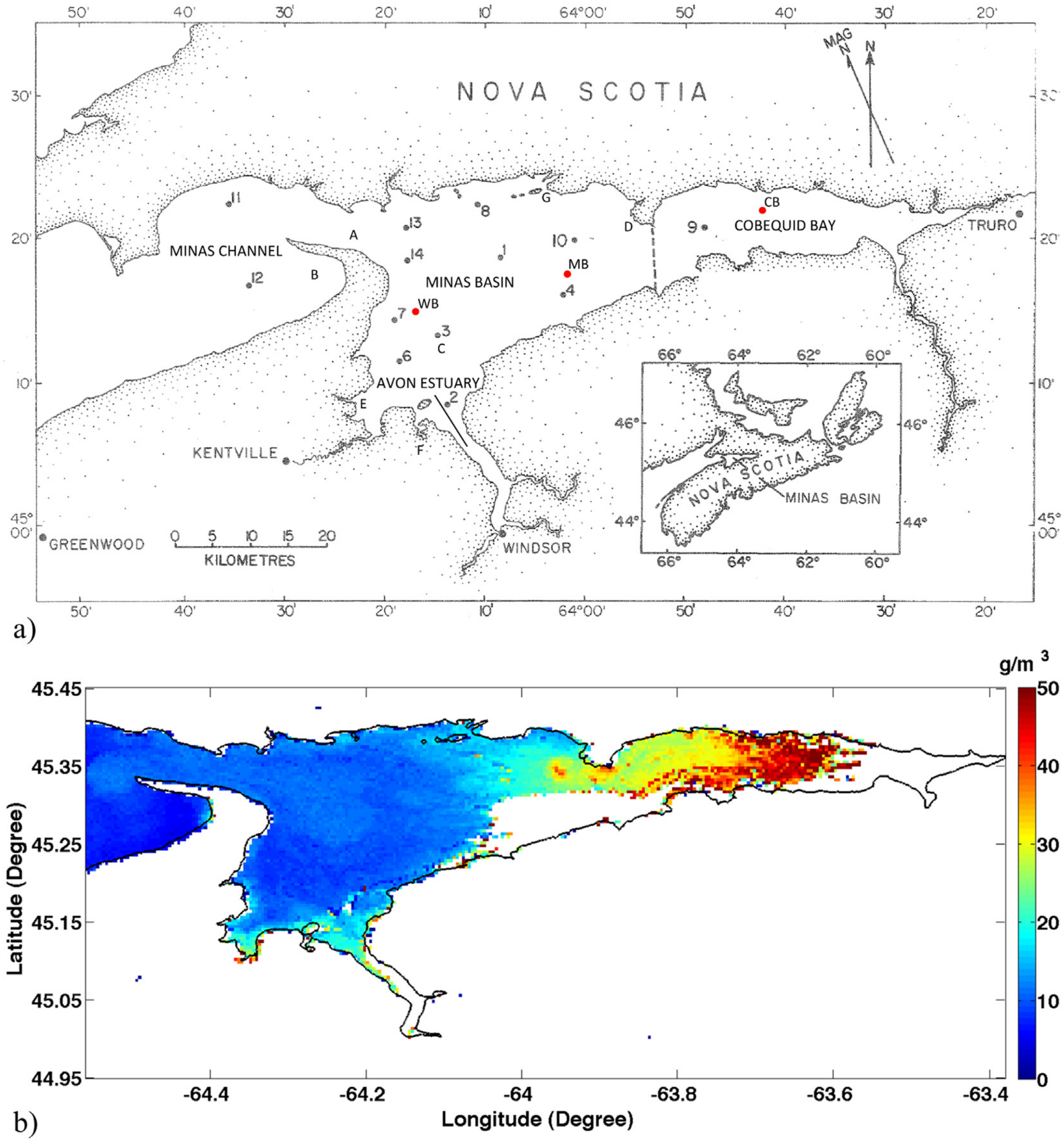

Fig. 1. a: Map of Minas Basin, Nova Scotia, Canada. A-Minas Passage, B-Scot's Bay, C-Windsor Bay, D-Economy Point, E-Cornwallis Estuary, F-Gaspereau Estuary, G-Five Islands (modified from Amos and Joice, 1977). *In situ* survey locations during 1975–76 are indicated at 1–14. Red dots are MERIS observation sites. b: Instantaneous total suspended matter (TSM; g/m^3) derived from a MERIS image in Minas Basin on 1506 GMT, February 10th, 2010.

of TSM made in Minas Basin include collection of suspended sediment samples from moorings and cruise surveys. The TSM concentration in the Bay of Fundy ranges from 0.2 to 30.4 g/m^3 with an average of 6.6 g/m^3, and concentration ranges from approximately 20 g/m^3 to 200 g/m^3 in Minas Basin (Amos and Alfoldi, 1979). Satellite-based estimates of water quality complement conventional monitoring techniques and have found widespread applications. Ocean color observations from space can produce nearly daily synoptic views of the distribution of water substances and concentrations with large spatial and temporal coverage, which is not available from other sources (Shen et al., 2010a). Remote sensing of TSM in very turbid waters (e.g., Changjiang estuary and the Bay of Fundy) is quite challenging due to the difficulty of atmospheric correction over turbid water and the empirical nature of the retrieval algorithms, which are limited to a specific range of concentrations, areas and seasons (Shen et al., 2010b).

Numerical models can be used to simulate various fundamental physical conditions of the coastal environment such as water height, currents and sediment processes. Wu et al. (2011) described the sediment transport in Minas Basin, including bed load and suspended particulate load, and evaluated the model against independent remote sensing images. Generally, the comparison between the model results and "observed" transport of suspended load showed reasonable agreement. The "observed" transport of suspended load was calculated using the MERIS TSM concentration and total velocity from hydrodynamic model. The FVCOM model used by Wu et al. (2011) appeared to overestimate the transport in Minas Basin and underestimate it in Cobequid Bay, indicating that the results are sensitive to the model input parameters. Mulligan et al. (2013) used the Delft3D model to examine the changes in currents and suspended sediments in Minas Basin.

In this study, *in situ* measurements, satellite observations and numerical modelling are used to advance the description and understanding of the spatial-temporal variability of surficial TSM over Minas Basin in the Bay of Fundy. The focus of the study emerged from recent research into seasonal changes in TSM and mudflat erodibility in the Minas Basin. Specifically, Wu et al. (2011) showed that TSM is higher in winter than in summer in the Minas Basin. Interestingly, Carrière-Garwood (2013) showed that erosion resistance of mudflats is higher in summer than in winter. Based on these observations, it is possible that the seasonal changes of erodibility of the mudflats could produce seasonal variability of TSM. The two objectives of this paper, therefore, are to expand the analysis of spatial patterns of seasonal variation in TSM in the Minas Basin and to explore the extent to which changes in erosion resistance of sediment on tidal flats can explain observed changes in TSM.

2. Materials and methods

2.1. MERIS satellite observations

MERIS satellite data are available from the European Space Agency (ESA) website, for the period from 2002 to 2012. MERIS has a higher spectral resolution, signal-to-noise ratio and spatial resolution than other sensors, such as Sea-viewing Wide Field-of-view Sensor (SeaWiFS) or the Moderate Resolution Imaging Spectroradiometer (MODIS) (Bourg et al., 2002). The MERIS Full Resolution (FR, 300 m) Level 2 images derived with MEGS 7.4 (MERIS Ground Segment prototype processor) were acquired in the inner Bay of Fundy over the period of May 2008 to July 2011. In general, TSM is defined as all matter (organic and inorganic) that stays on a Whatman GF/F glass fiber filter with an approximate pore size of 0.7 μm (Eleveld et al., 2008). The MERIS TSM product in this work is an estimate of total non-chlorophyllous suspended matter, which is assumed to be inorganic sediment solely composed of non-absorbing mineral particles, so a more appropriate name would be 'total suspended mineral matter'. Given the large concentrations of mineral matter in Minas Basin, it is assumed herein that total suspended matter is approximately equal to total suspended mineral matter, and the acronym *TSM* is applied to the MERIS TSM, to *in situ* observations, and to model output. The non-chlorophyllous suspended matter concentration is characterized by its high scattering coefficient at 550 nm [b_p (550); m^{-1})], and was converted from optical units (backscatter in m^{-1}) to geophysical units (concentration in g/m^3) using a fixed conversion factor derived from *in situ* optical measurements and water samples (Doerffer and Schiller, 2007). The accuracy of the conversion factor can be affected by different TSM composition (Babin et al., 2003; Bowers et al., 2009). The MERIS algorithm advanced theoretical basis documents are available on https://earth.esa.int/instruments/meris/atbd/atbd_2.12.pdf.

MERIS images were cropped to cover only the Minas Basin. An image was taken on 10th February 2010 in a relatively clear atmosphere (Fig. 1b) shows a typical spatial pattern of TSM, with elevated concentrations in the shallow waters that fringe the Basin and lower concentrations in the center of the Basin. For each of the TSM images, SeaDAS and IDL software packages were used to determine the spatial average TSM concentration with a small pixel box (3 × 3 pixels; ~1 km^2). Time series of TSM values in that small pixel box were generated through the whole period. The algorithm for MERIS satellite estimates of TSM concentrations is reliable for low to moderate concentration (1–50 g/m^3, Shen et al., 2010b; Doerffer and Schiller, 2007). MERIS TSM products were used in a previous study to assess TSM levels within the Northumberland Strait located to the north of Minas Basin (Bugden et al., 2007). That study examined the accuracy of the MERIS TSM calibration by comparing MERIS with *in situ* surface observations on October 17th, 2006. MERIS TSM was a mean value over a 1-km^2 area closest to the sample sites, and Bugden et al. (2007) indicated that MERIS reliably estimated TSM concentrations in their region. The Bugden et al. (2007) comparison of estimated versus observed TSM was conducted for relatively low TSM concentrations; so it is important to assess, at least qualitatively, the applicability of MERIS data to estimate high concentrations of TSM that can occur in Minas Basin.

2.2. In situ data

Amos and Joyce (1977) presented *in situ* TSM concentrations in Minas Basin, including concentrations as a function of location, depth, and time. There were 11 sites located in Minas Basin (Fig. 1a). The surface (0–1 m) TSM concentrations are listed in Table 1. The reported TSM values ranged from 3.5 to 26.9 g/m^3 in Minas Basin. *In situ* TSM concentrations were compared with MERIS satellite observations to check that the *in situ* measurements and MERIS estimates of TSM were of comparable magnitude.

2.3. Delft3D model

Delft3D is a numerical model capable simulating circulation, sediment transport, waves, water quality and morphological changes in coastal waters (Sutherland et al., 2004). Lesser et al. (2004) provide a detailed description of the model underlying equations and show that the coupled hydrodynamic and sediment modules are capable of simulating many of the important processes that are relevant in coastal environments, including suspended sediment transport.

The model computes the hydrodynamics based on the fluid momentum equations that depend on bathymetry, subject to initial conditions and boundary conditions. The transport of fine suspended sediment is calculated from the local instantaneous flow conditions (Borsje et al., 2008) based on the advection–diffusion equation (Equation (1)). Delft3D categorizes the different sediments as either 'cohesive', 'non-cohesive' or 'bed load'. As this study focuses on suspended sediments at the sea surface, this section deals primarily with 'cohesive', and only one fine sediment fraction is used. The three-dimensional suspended sediment transport is calculated by solving the following advection-diffusion equation for each control volume for one sediment fraction (WL|Delft Hydraulics, 2006):

$$\frac{\partial c}{\partial t}+\underbrace{\frac{\partial uc}{\partial x}+\frac{\partial vc}{\partial y}+\frac{\partial (w-w_s)c}{\partial z}}_{\text{advection}}-\underbrace{\frac{\partial}{\partial x}\left(\varepsilon_{s,x}\frac{\partial c}{\partial x}\right)-\frac{\partial}{\partial y}\left(\varepsilon_{s,y}\frac{\partial c}{\partial y}\right)-\frac{\partial}{\partial z}\left(\varepsilon_{s,z}\frac{\partial c}{\partial z}\right)}_{\text{diffusion}}=0 \quad (1)$$

where c is mass concentration of sediment, u, v, w are flow velocity components, $\varepsilon_{s,x}$, $\varepsilon_{s,y}$, $\varepsilon_{s,z}$ are eddy diffusivities in three directions, and w_s is settling velocity of suspended sediment. In Equation (1), the geographic coordinate system of velocity is defined as positive eastwards, northwards and upwards. The settling velocity w_s is positive downwards, so the sign of this term is negative. The

Table 1
The mean and standard deviation (SD) of surface TSM (0–1 m) for various dates in 1975–76 at Amos and Joyce (1977) sites in Minas Basin.

Station	Mean TSM (g/m^3)	SD
1	6.440	3.220
2	26.994	13.497
3	7.315	3.658
4	6.143	3.071
6	12.078	6.039
7	4.528	2.264
8	3.506	1.753
9	8.471	4.235
10	11.409	5.705
13	4.785	2.392
14	5.459	2.729

exchange of material through the bottom boundary is modelled by the fluxes between the bottom-most water layer and the bed as defined by:

$$-w_s c - \varepsilon_{s,z}\frac{\partial c}{\partial z} = D - E, \quad \text{at } z = z_b \tag{2}$$

where D represents deposition flux of suspended matter, E is re-suspension flux, and z_b is the location of the bed in the water column. For the mud sediment fraction, the deposition (D) and erosion (E) terms are calculated with the Partheniades-Krone formulations (Lesser et al., 2004):

$$E = M \cdot S(\tau_{cw}, \tau_{e\_crit}) \tag{3}$$

$$D = w_s \cdot c_b \cdot S(\tau_{cw}, \tau_{d\_crit}) \tag{4}$$

where M is first order erosion rate (erosion parameter), τ_{cw} is maximum bed shear stress due to current and waves, c_b is average sediment concentration in the near bottom computational layer, τ_{e_crit} is critical bed shear stress for erosion and τ_{d_crit} is critical bed shear stress for deposition. $S(\tau_{cw}, \tau_{e\_crit})$ and $S(\tau_{cw}, \tau_{d\_crit})$ are erosion and deposition step functions respectively, which are defined as

$$S(\tau_{cw}, \tau_{e\_crit}) = \left(\frac{\tau_{cw}}{\tau_{e\_crit}} - 1\right), \quad \text{when} \tau_{cw} > \tau_{e\_crit},$$
$$= 0, \quad \text{when } \tau_{cw} \le \tau_{e\_crit}.$$

$$S(\tau_{cw}, \tau_{d\_crit}) = \left(1 - \frac{\tau_{cw}}{\tau_{d\_crit}}\right), \quad \text{when} \tau_{cw} < \tau_{d\_crit},$$
$$= 0, \quad \text{when} \tau_{cw} \ge \tau_{d\_crit}.$$

The vertical sediment transport is mainly affected by the sedimentation and re-suspension flux, which are affected by the settling velocity (w_s) and erosion parameter (M) respectively. In the model, the bottom shear stress (τ_{cw}) plays an essential role in defining whether or not sedimentation of suspended particles or erosion of bed material will occur. Sedimentation takes place when the bottom shear stress drops below a critical value (τ_{d_crit}) and erosion occurs when the bottom shear stress exceeds the critical value for re-suspension (τ_{e_crit}). The bottom shear stress is based on the shear stress due to currents and waves (Borsje et al., 2008), but only tidal current effects are considered in the model simulations.

In this study, a boundary-fitted grid in spherical coordinates has been developed for Minas Basin covering a domain of approximately 110 km in the east-west direction and 45 km in the north-south direction. An open boundary across Minas Channel (18 km west of Cape Split) controls tidal water level elevations and allows inflow and outflow. The circulation model for Minas Basin has a horizontal resolution of 200 m, and the vertical resolution is variable with 10-layers in topography-following coordinates. The sediment included in the model is cohesive fine sediment only. The parameters required to model cohesive sediment include critical bed shear stresses for erosion τ_{e_crit} and deposition τ_{d_crit}, the particle settling velocity w_s and the erosion parameter M. The critical stress for bed erosion is a complex variable, dependent on the antecedent stress history of sediment and on the *in situ* bulk sediment properties, whereas the critical deposition stress is a function of grain properties of the suspended material, concentrations and salinity (Amos and Mosher, 1985). Amos et al. (1992) measured *in situ* bed shear stresses for erosion (τ_{e_crit}) of up to 0.1–7.5 N/m^2 (in July and August, 1989–1990) across the 2.5 km wide mudflat, which notably is 1–2 order of magnitude larger than for other studies (e.g. Greenberg and Amos (1983) use 0.1–0.2 N/m^2) and for other estuaries (Houwing, 1999). Amos (1985) used the values of τ_{d_crit} in the range from 0.121 to 0.100 N/m^2 in testing the sediment accumulation rates on Windsor Bay. They found that the use of τ_{d_crit} of Creutzberg & Postma produced the closest approximation to the observations made in the field (Amos and Mosher, 1985). For the fine suspended sediment, the settling velocity (w_s) varies in time and space as a result of flocculation (Winterwerp, 2002). The settling velocity for the surface sample was set to 0.4 mm/s in Amos's (1985) study. Hu et al. (2009) set up the Delft3D-FLOW for a 2D/3D hydrodynamic and sediment transport in the Yangtze Estuary, China, the fifth largest river in the world in terms of suspended sediment load. The erosion parameter that Hu et al. (2009) used was around 2.5 × 10^{-6} kg/m^2/s with spatial variation. In the present study, τ_{e_crit} was varied from 1 to 2 N/m^2 and τ_{d_crit} was set to 0.2 N/m^2. The settling velocity was varied from 0.1 to 0.5 mm/s, corresponding to a grain size of less than 100 μm in agreement with Amos (1985). The erosion parameter M was varied from 5 × 10^{-6} to 5 × 10^{-5} kg/m^2/s.

The seabed sediment distribution was specified as a bi-modal distribution with an initial seabed of cohesive mud in water depths of 10 m and less (mean sea level) and no sediment in depths greater than 10 m. This parameterization is justified by the focus here on fine suspended sediment, which does not derive from coarser sediment typical of deeper waters in the Basin. This description generally matches the distribution of mud in the Basin (Dalrymple et al., 1990). The model was initialized from rest with 0 g/m^3 sediment, and 6 days were required for spin-up time of the tidal currents and suspended sediment concentrations prior to analysis of the results. The amplitude and phase of the M2 tidal constituent (12.42 h period) were specified at the model open boundary. This is the dominant tidal constituent over the region and can be considered to be representative of general tidal forcing (Greenberg and Amos, 1983).

The model skill was assessed by comparing predictions of the flow velocity and sediment concentration to observations. Hydrodynamic validation was conducted by comparison of velocity components (u, v) with the ADCP (Acoustic Doppler Current Profilers) observations near the centre of Minas Basin. Model results agreed with the observed tidal amplitudes and phases (Mulligan et al., 2013). Performance of the sediment model was assessed by comparison of modelled TSM concentration patterns with satellite-derived TSM patterns at the surface layer in Minas Basin.

2.4. Methodology

2.4.1. Autocorrelation analysis

MERIS TSM products are typically unequally spaced in time, which makes spectral analysis difficult. Unequal spacing arises because satellite performance depends on widely varying conditions, such as cloud cover. To deal with this issue, a variogram was used for determining the temporal correlation of observations. For a stationary random process $\{Y(t)\}$, the distribution of $Y(t)-Y(t-k)$ does not depend on t. The mathematical definition of the variogram, $V(k)$, is.

$$V(k) = \frac{1}{2}E\left[\{Y(t) - Y(t-k)\}^2\right] \quad (5)$$

where k is a time lag, and $E(x)$ denotes the expected value of x. For a series $\{y(t_i): i = 1, \ldots, n\}$, a plot of the quantities $v_{ij}=½\{y(t_i)-y(t_j)\}^2$ against $k_{ij}=t_i-t_j$ for all $½n(n-1)$ distinct pairs of observations is called the empirical semi-variogram (Diggle, 1990). The time lag k is plotted along the horizontal axis and the value of the semi-variogram along the vertical. The k starts at zero, since the lag k is always positive. The v_{ij} axis also starts at zero by definition.

Since the observations were highly irregular in time, there were more than one v_{ij} corresponding to a particular value of k_{ij}. The sample variogram was simplified by replacing all v_{ij} by their mean value, $\overline{V(k)}$, leading to a desirable reduction in the amount scatter in the sample variogram (Diggle, 1990). Then, $\overline{V(k)}$ was normalized by the variance of the time series, σ^2, producing the normalized sample variogram:

$$V_v\left(k\right) = \overline{V(k)}\Big/\sigma^2 \quad (6)$$

The normalization by the variance is useful because $\overline{V(k)}$ can be small when large values of Y are similar or because the absolute values of Y are small. The normalization emphasizes lags for which correlation is high. When the $V_v(k)$ value is close to the zero, the time series is highly auto-correlated at a time lag k. Because high autocorrelation is indicative of periodicity, calculation of the variogram can be used to identify the dominant time scales of variability in TSM. The temporal variogram analysis was applied to the TSM time series at each pixel box in Minas Basin. The analysis was used to assess how the degree of autocorrelation varies as a function of geographic location in the Basin. The benefit of this approach is that it creates spatial maps of where seasonal signals were strongest, providing an effective way to carry out a model-data comparison in the Basin.

2.4.2. Relative difference

Comparison using the relative difference (RD) directly capitalizes on the spatial coincidence between grid-based data maps. It simply compares the corresponding values at each grid position. The RD were calculated with the following equation (Berry, 1999):

$$\mathrm{RD} = \left[\frac{[\mathrm{map1_{value}} - \mathrm{map2_{value}}]}{\mathrm{map2_{value}}}\right]*100 \quad (7)$$

This method is easy to interpret, uses the entire data range, and depicts relative differences geographically. In this study, the $\mathrm{map1_{value}}$ indicates the simulated model TSM concentration, and $\mathrm{map2_{value}}$ indicates the observed satellite TSM concentration. When the RD was larger than 0%, the modelled TSM was larger than the satellite estimated value; otherwise the modelled TSM was less than or equal to the satellite estimate.

3. Results

3.1. Seasonal variability of satellite TSM concentration

Three sites in the Minas Basin are useful for portraying the range of temporal autocorrelation in TSM. These three sites are named MB (Minas Basin), WB (Windsor Bay) and CB (Cobequid Bay) (Fig. 1a). The mean depths of these three stations are 18.4, 32.7 and 9.9 m. The tidal range is 13.9 m, so all stations are covered with water during all tidal stages. Time series of satellite-derived TSM concentration showed a clear annual cycle at MB near the centre of Minas Basin (Fig. 2a). The peak values of TSM concentration were around 40–50 g/m^3 in mid-winter (March and April), and different for each year. The peaks are equivalent within the error bars of ~ +/− 5 g/m^3. The lower values of TSM concentration were around 0–10 g/m^3 in mid-summer (July and August) (Table 2). The TSM concentrations were variable at this location over the winter. However, the TSM concentrations were relatively stable during the summer, generally remaining between 0 and 10 g/m^3. The sample variogram of the TSM time series at MB in the central part of Minas Basin highlights the yearly cycle (Fig. 2b). Smaller sample variogram values indicate stronger autocorrelation. The sample variogram shows that concentrations were least correlated at time lags of approximately 6, 18 and 30 months (~180, 540 and 900 days), and most correlated at time lags of approximately 12, 24 and 36 months (~360, 720 and 1080 days). Values of $V_v(k)$ had more variance when time lag k was over 900 days because, given the length of the time series, there were few observations with lags between them that were this large. The factors responsible for the annual cycle are further discussed in section 4.2.

The TSM concentration at WB (Fig. 2c) also varied annually, but concentrations were lower than in the centre of Minas Basin. The maximum TSM concentration was approximately 20 g/m^3 in late winter at position WB, and the concentration was between 0 and 5 g/m^3 in mid-summer (Table 2). The variogram of the TSM time series at WB is similar to the variogram at MB, revealing strong correlation at lags of 12, 24 and 36 months (Fig. 2d). The TSM concentrations at CB did not vary annually, and they fluctuated considerably during the entire period. The TSM values ranged from 0 to 90 g/m^3 (Fig. 2e) (Table 2). The sample variogram of the TSM time series at CB shows no correlation at annual (or any other) time scales (Fig. 2f).

An alternative method for examining the annual variability in TSM concentration is to examine maps of the mean TSM in each pixel box in late summer and winter (Fig. 3). The summer period is defined here to include just two months, July and August. The winter period contains February and March data. In 2009 there were 26 satellite images in summer and 38 images in winter. Most of the mean TSM values were between 0 and 10 g/m^3 in the central Minas Basin and between 10 and 20 g/m^3 in Cobequid Bay and Windsor Bay in summer. In winter, the TSM concentrations increased eastward and southward from the mouth of Minas Passage, and the TSM values were between 15 and 35 g/m^3 in the central Minas Basin, and between 30 and 50 g/m^3 in Cobequid Bay and Windsor Bay. The seasonal changes in satellite TSM concentrations were estimated by dividing the differences between summer and winter TSM concentrations by the winter TSM concentrations for each pixel box over the entire area (Equation (7)). Using TSM in winter as $map2_{value}$, satellite mean TSM concentrations showed seasonal variability in Minas Basin in 2009 (Fig. 4). Because the TSM concentrations in winter were higher than in summer, the RD were negative. The summer-winter differences were largest in the northern Basin, giving the largest negative RD at −90%.

3.2. Strength of annual signal

The spatial pattern of normalized sample variograms $V_v(k)$ at 1-year lag is examined to understand the geographic distribution of the strength of the annual signal of satellite TSM concentration. As indicated earlier, smaller sample variogram values indicate stronger autocorrelation. The minimum value of sample variograms between time lag k of 365 ± 30 days (1 year) was plotted (Fig. 5).

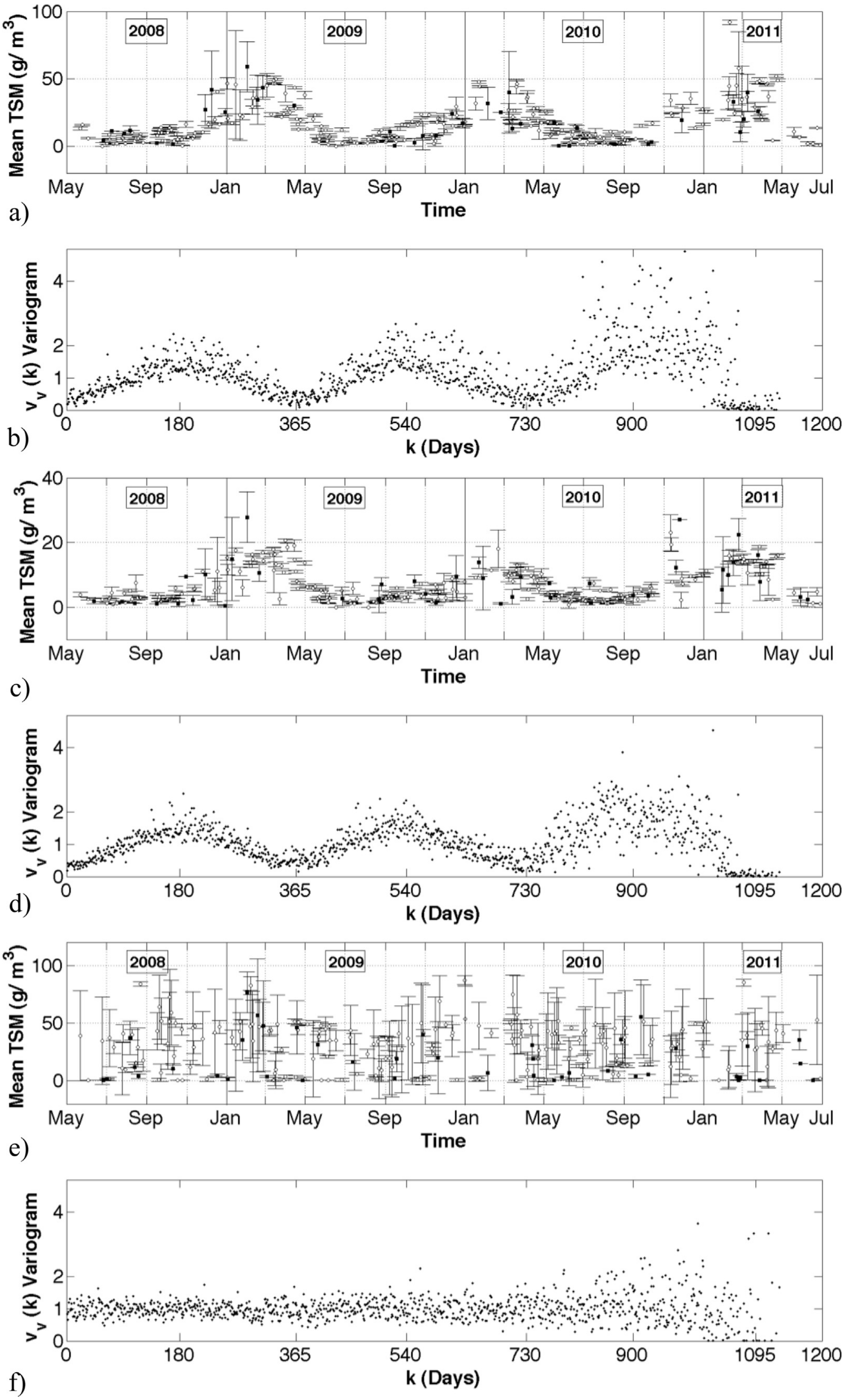

Fig. 2. Time series of TSM concentration derived from the MERIS satellite: a) mean values of TSM concentration over a 1-km^2 pixel box (3×3 pixels) at MB in the centre of Minas Basin from May 2008 to July 2011; b) sample variograms of TSM at same location. In the top panel, an unfilled circle presents TSM data for which all nine pixels were used in the average, and a filled square indicates fewer than nine pixels were used. Error bars denote the standard deviation of TSM concentration values in the pixel box. In the bottom panel, smaller values indicate stronger autocorrelation. The normalized variogram shows that concentrations are least correlated at time lag of approximately 180 days. c) and d) are calculated from the time series at site WB. e) and f) are calculated from the time series at site CB.

Table 2
Summary of site locations and TSM concentration in Minas Basin.

Site name (initial)	Latitude	Longitude	Max. (g/m^3)	Min. (g/m^3)	Figure
Minas Basin (MB)	45.2962°	−64.0186°	40–50	0–10	2a
Windsor Bay (WB)	45.2731°	−64.2637°	20	0–5	2c
Cobequid Bay (CB)	45.3654°	−63.6892°	0–90		2e

Over the central Minas Basin, the $V_v(k)$ ranged between 0.05 and 0.15 indicating that the satellite TSM displays a stronger annual signal here. The annual signal was weak in Cobequid Bay, southern Windsor Bay and around coastlines. The black dots around the shorelines are noise. The white (no signal areas) generally had high but variable TSM concentrations throughout the year. The warm color areas shown in Fig. 5 had the higher TSM seasonal variability.

3.3. Delft3D model

The Delft3D model results from the last 2 days of each model run were used to calculate the time-mean fields of TSM concentration. The values of critical bed shear stress for erosion, τ_{e_crit}, and deposition, τ_{d_crit}, the erosion parameter, M, and particle settling velocity, w_s, were varied among simulations (Table 3). Runs C2 and C3 were the best able to reproduce winter and summer TSM

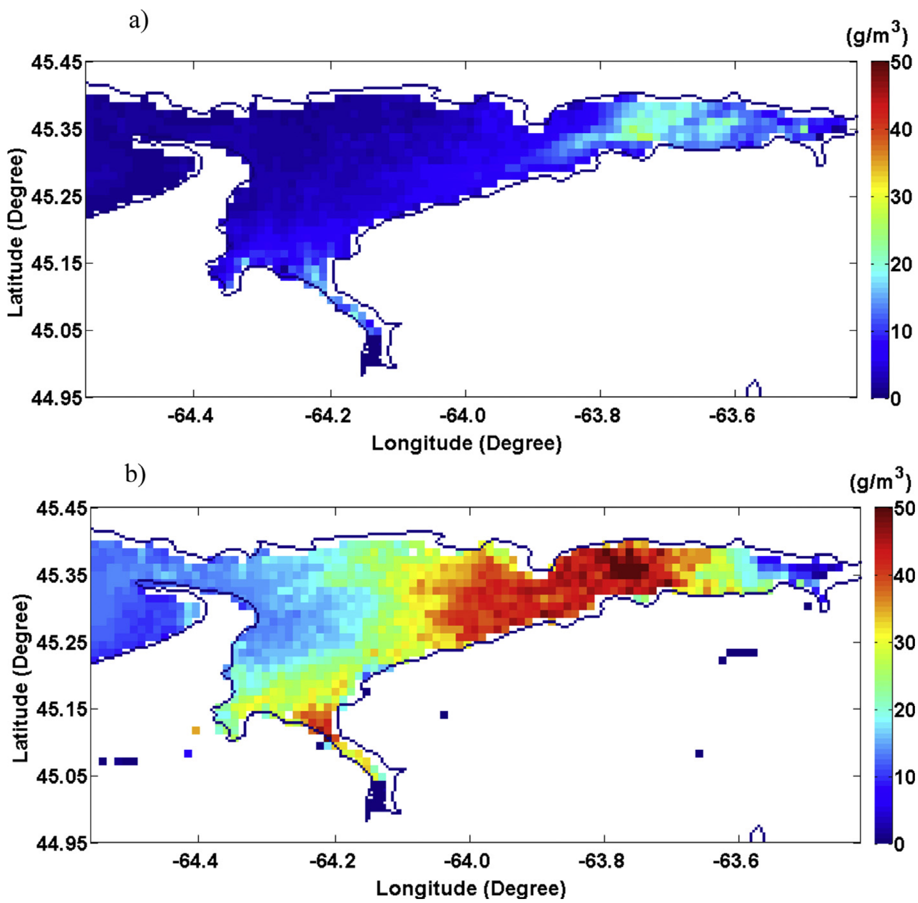

Fig. 3. Distributions of time-averaged satellite-derived mean TSM concentration estimated from MERIS images during a) Summer and b) Winter 2009 in Minas Basin. Largest concentrations, shown in warm colours, occurred in Cobequid Bay and in Windsor Bay. Smallest concentrations occurred in Minas Passage. Over the basin, the mean TSM concentrations were higher in winter than in summer.

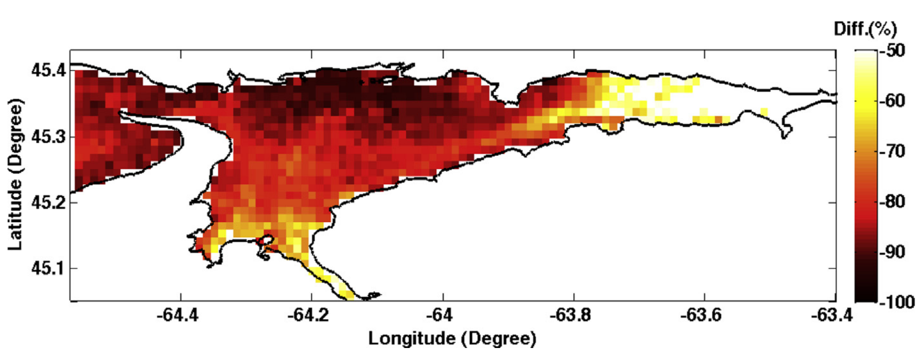

Fig. 4. Satellite TSM concentration seasonal differences between summer and winter, normalized by winter values, in 2009 in Minas Basin.

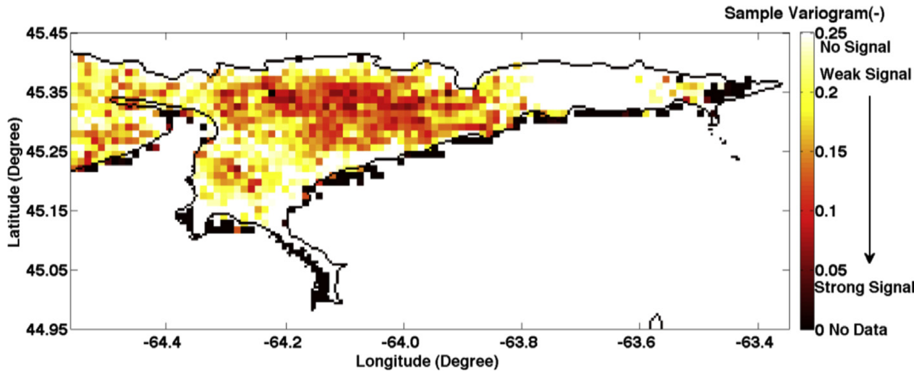

Fig. 5. Distributions of estimated annual change in TSM concentration observed by the MERIS satellite, where normalized sample variogram is the minimum value during $k = \pm 30$ days of a year. Lower values indicate larger annual variation and are represented by darker colours.

concentration, respectively. For Run_C2, settling velocity had a high value, critical erosion shear stress had a low value, and the erosion parameter had an intermediate value. Modelled TSM concentrations in the Basin were similar to those observed in winter (Figs. 3a and 6a). Suspended sediment concentrations were approximately 50 g/m^3 in Cobequid Bay and Windsor Bay. Suspended sediment concentrations ranged from 15 to 30 g/m^3 in the central part of Minas Basin. For Run_C3, settling velocity had an intermediate value, critical erosion shear stress had a low value, as did the erosion parameter. Modelled TSM concentrations in the Basin were similar to those observed in summer (Figs. 3b and 6b). Throughout the entire Basin, suspended sediment concentrations were below 20 g/m^3. TSM concentrations in shallow areas were higher than in the central Basin.

3.4. Satellite versus model TSM concentration

The summer of 2010 and winter of 2009 were chosen for a quantitative comparison between the model results and observations because these two seasons had the largest numbers of satellite images, increasing confidence in the satellite estimates of TSM concentration. The light to white color in the maps indicates that the RD values were between ±50%, which is defined in this work as an acceptable difference (Fig. 7). Based on the results presented in Table 1, the variability in observed TSM at a site is ±50%, so this value was selected as a reasonable threshold of agreement between the simulated and observed TSM (discussed further in section 4.3). The fraction of pixel boxes that had RD in the range of ±50% is termed the "White ratio". Larger white ratios indicate better agreement between model and satellite TSM concentrations. The largest white ratio for winter 2009 was Run_C2 and for summer 2010 was Run_C3, which were respectively equal to 49.76% and 49.47% (Table 3). Sediment distributions for these runs appear in Fig. 6.

Model runs A4, B4 and C3 had the largest white ratios in summer (Fig. 7, Table 3). These runs shared the common feature of using a smaller value for the erosion rate. The spatial variation was different for each simulation for the same season. Run_A4 showed better skill at predicting TSM concentration in Cobequid Bay than Run_B4 and Run_C3, but it overestimated TSM concentration in most areas of the central Minas Basin and southern Windsor Bay. Larger settling velocities in runs B4 (0.5 mm/s) and C3 (0.4 mm/s) resulted in less sediment in suspension in the deeper Minas Basin, producing better agreement in this area. They also, however, underpredicted concentration over the shallower Cobequid Bay.

Model runs A1, C2 and C4 had the highest white ratios for winter, again just under 50% (Fig. 7, Table 3). These runs shared the common feature of using a larger value for the erosion rate. The spatial variation was different for each simulation for the same season. Run_A1 showed less skill at predicting TSM in Cobequid Bay than Run_C2 and Run_C4, and it overestimated TSM concentration in the eastern end of Cobequid Bay. Smaller erosion parameters in runs C2 (4×10^{-5} kg/m^2/s) and C4 (4.5×10^{-5} kg/m^2/s) resulted in less sediment than Run_A1 (5×10^{-5} kg/m^2/s) in suspension in the deeper Minas Basin, producing better agreement in this area. They also, however, caused over-prediction of concentration over the shallow Cobequid Bay, over a smaller area of Windsor Bay and at Five Islands. Additionally, they under-predicted TSM in the Minas Passage.

In summary, model parameters that produced a good agreement between modelled and satellite-derived TSM concentration in the central Minas Basin also produced TSM that were different from satellite-derived estimates in shallow areas. In Cobequid and Windsor Bays, modelled TSM concentrations were higher than satellite-derived estimates in winter. For all model simulations, the TSM concentrations were lower than satellite-derived TSM at Minas Passage. This simplified modelling approach, by varying the sediment parameters in each run, suggests that the sediment parameters vary in space and time, so a perfect match between model and data will be difficult to achieve in all parts of the Basin.

Two primary results emerged from the analysis and comparison of modelled and satellite-derived TSM concentration in Minas Basin. First, satellite-derived TSM concentration varied annually, with lower TSM in late summer and higher TSM in late winter. The annual signal was strongest in the central Minas Basin and weaker

Table 3
List of Delft3D model processing parameters and corresponding white ratio for each run.

Run number	w_s	τ_{d_crit}	τ_{e_crit}	Erosion parameter	White Ratio:(|RD|<50%)/total	
	[mm/s]	[N/m^2]	[N/m^2]	[kg/m^2/s]	2009 Winter	2010 Summer
A1	0.1	0.2	2	5×10^{-5}	41.68%	–
A2	0.1	0.2	2	5×10^{-6}	–	15.16%
A3	0.1	0.2	1	5×10^{-5}	11.41%	–
A4	0.1	0.2	1	5×10^{-6}	–	44.91%
B1	0.5	0.2	2	5×10^{-5}	25.70%	35.62%
B2	0.5	0.2	2	5×10^{-6}	–	2.06%
B3	0.5	0.2	1	5×10^{-5}	39.72%	–
B4	0.5	0.2	1	5×10^{-6}	–	44.52%
C1	0.1	0.2	2	4×10^{-5}	36.48%	–
C2	0.5	0.2	1	4×10^{-5}	49.76%	–
C3	0.4	0.2	1	5×10^{-6}	–	49.47%
C4	0.5	0.2	1	4.5×10^{-5}	44.93%	–

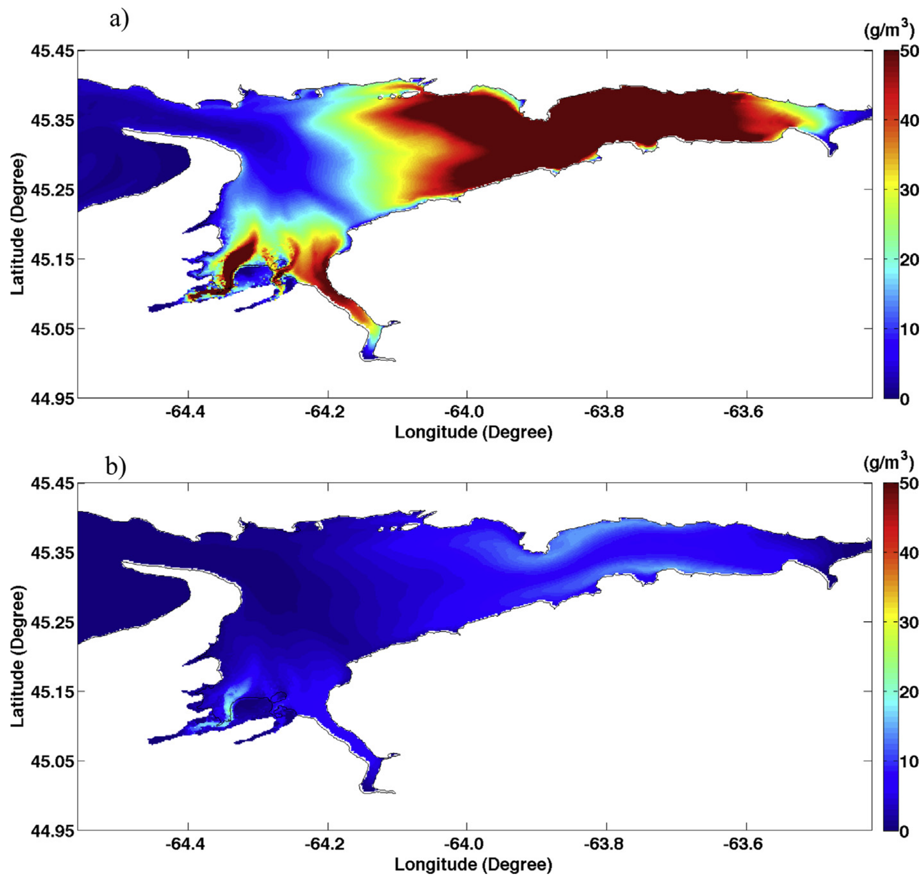

Fig. 6. The time-mean simulated TSM concentration with parameters: a) $w_s = 0.5$ mm/s, $\tau_{e\_crit} = 1$ N/m^2 and $M = 4 \times 10^{-5}$ kg/m^2/s; b) $w_s = 0.4$ mm/s, $\tau_{e\_crit} = 1$ N/m^2 and $M = 5 \times 10^{-6}$ kg/m^2/s in Minas Basin.

in the shallow areas of Cobequid and Windsor Bays. The model reproduced the annual variation in TSM concentration by increasing the erosion rate by an order of magnitude for winter simulations. Second, seasonal changes in modelled and satellite-derived TSM concentration did not match over the shallow areas, indicating either that satellite-derived TSM or the modelled TSM were not accurate in these areas. These two results are discussed in more detail in the following sections.

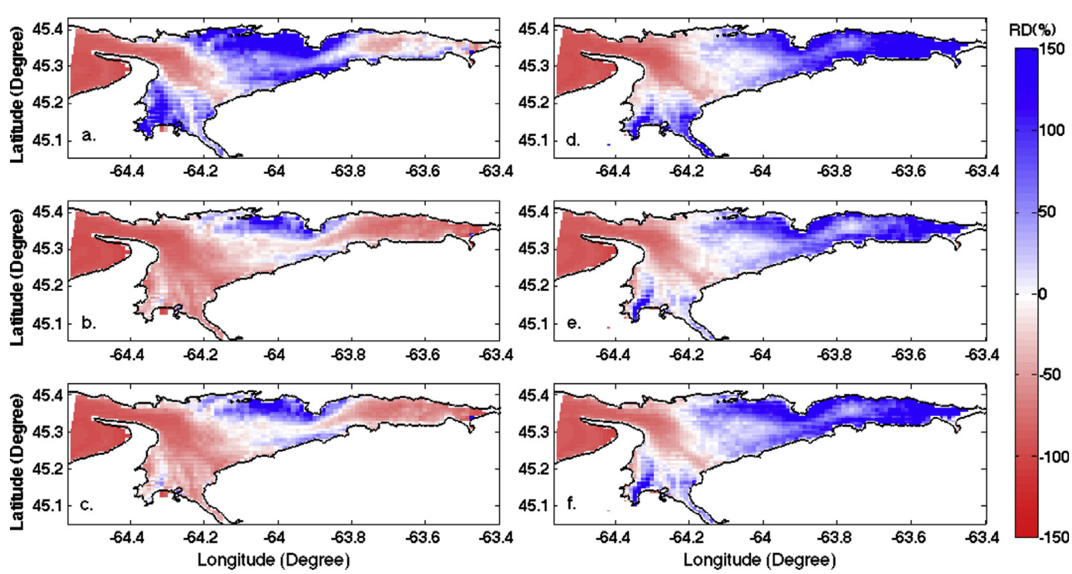

Fig. 7. Quantitative comparison between model and satellite-derived TSM concentration during summer 2010 with a) $w_s = 0.1$ mm/s; b) $w_s = 0.5$ mm/s; c) $w_s = 0.4$ mm/s. Quantitative comparison between model and satellite-derived TSM concentration during winter 2009 with d) $M = 5 \times 10^{-5}$ kg/m^2/s; e) $M = 4 \times 10^{-5}$ kg/m^2/s; f) $M = 4.5 \times 10^{-5}$ kg/m^2/s.

4. Discussion

4.1. Comparison of satellite-derived and in situ TSM concentration

To investigate the accuracy of the satellite-derived TSM concentration in Minas Basin, the observations of satellite-derived TSM concentrations were compared with *in situ* observations. The summer 2010 observations of satellite-derived TSM concentrations and *in situ* TSM concentrations were compared at several locations of the Basin. A log–log scatterplot of TSM estimated by satellite versus *in situ* TSM shows that points fall close to a 1:1 line (Fig. 8) despite the fact that the *in situ* and satellite observations are widely separated in time. Note that the satellite-derived TSM and the measured *in situ* TSM were collected in the same season (summer). Generally, the satellite-derived TSM concentrations have similar magnitude as *in situ* observations in Minas Basin observation points. However, the *in situ* TSM concentrations are generally higher than satellite-derived TSM. These results may indicate that satellite-derived TSM are underestimates in summer.

4.2. Causes for annual cycle of TSM concentration

The factors responsible for the annual cycle of TSM variability are unclear, but several possible mechanisms exist. Annual cycles in TSM concentration may be caused by higher erosion rates in the winter. Destruction of sediment biofilms may reduce sediment adhesion and induce the higher erosion rates in the winter. Borsje et al. (2008) showed that the small-scale biological activity on the bottom of the seabed has significant influence on the dynamics of cohesive sediment on a large spatial and temporal scale. They used the process-based sediment transport module of Delft3D to assess effects of biology on the Western Wadden Sea. The modelling results indicated that the seasonal variation in the sediment concentration is caused by wind and biological activity. The Western Wadden Sea is a tidal basin similar to Minas Basin, so it's reasonable to consider that biological activity also has significant influence on erosion rate in Minas Basin. Wave erosion of Triassic sandstone cliffs that surround the shoreline supplies an abundance of sand into Minas Basin (Thomas, 1976; Stea, 2003). Amos (1984) estimated that a total of 3.1 $\times$ 10^6 m^3 of sand is introduced to the system annually from erosion of the cliffs. The cliffs erode supplying 1 $\times$ 10^6 m^3 per annum of finer-grained sediment, while a further source of fine-grained material is derived largely from seabed erosion (Amos and Long, 1980). Erosion rates are larger during storms, which are stronger in the winter. Amos and Long (1980) and Greenberg and Amos (1983) argued that sediment concentration at any sites within the Minas Basin is controlled by such processes as biological activity and wave stirring on the intertidal zone, rather than any other phenomena. Enhanced flocculation in the summer also could account for the decrease in suspended sediment concentration in that season. Flocculation increases the settling velocity of the fine-grained particles by several orders of magnitude (Hill et al., 2000; Mikkelsen et al., 2004), which would lower TSM concentration in the water column in summer.

The annual cycle of TSM concentration in Minas Basin was simulated by altering the erosion rate in Delft3D. This approach attributes the changes in TSM concentration to the effect of biofilms on sediment cohesion. The possibility that increased wave stress results in higher TSM concentration in winter has not been addressed with the model.

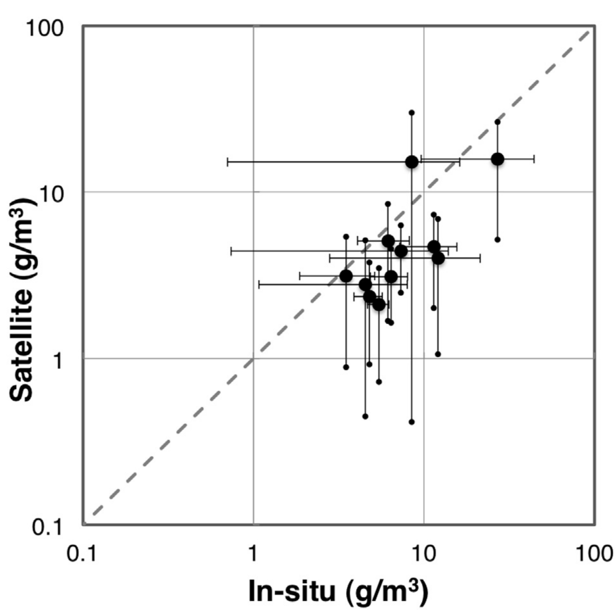

Fig. 8. Log–log scatter plot of TSM concentrations measured by satellite-derived (2010) and *in situ* (1975–76) measurements at Amos and Joyce (1977) sites in Minas Basin during summer (months June, July and August). Error bars indicate ±1 SD. The 1:1 line is shown in grey dash line.

4.3. Accuracy of satellite-derived vs. modelled TSM in shallow regions

The results show that, relative to the satellite-derived TSM concentration, the model underestimates TSM at Cobequid Bay and Windsor Bay in summer and overestimates TSM at shallow areas in winter. It is not clear whether the model or the observations are more accurate in the shallow areas.

4.3.1. Accuracy of satellite MERIS TSM concentration

The MERIS sensor may not resolve TSM concentration changes in shallow areas. The problems associated with remote sensing of TSM in coastal waters include difficult atmospheric corrections, confounding effects of phytoplankton, and light scatter from the seabed. The error of the concentration of a water constituent, such as TSM, derived from remote sensing data depends on several conditions. One important condition is that the accuracy of the input data, i.e. the water-leaving reflectance, which depends on errors in atmospheric correction. Atmospheric correction for optically shallow waters requires ancillary measurements at the time of image acquisition, which are often not possible on a routine basis. The unsolved problem of atmospheric corrections is the limiting factor for remote sensing of coastal waters (C. Mobley, personal communication). The water leaving radiance of shallow coastal waters may also be affected by the reflection of the seabed. Reflectance by sea bottom can be neglected when water depth is much more than signal depth. No bottom effect on water leaving radiance is considered when processing MERIS data (MERIS product handbook, 2006).

The Minas Basin area is an extremely complex optical environment. The turbid coastal water causes problems with the atmospheric corrections, as does absorption from non-algal particles. Wetting and drying of tidal flats in Cobequid Bay and Windsor Bay can lead to uncertainty and systematic errors in satellite estimates of TSM concentration. Parker et al. (2007) documented the extensive areas of intertidal mud flats in Minas Basin, owing to the high tidal range, coastal erosion and sediment washed in from the Salmon, Cornwallis, and Avon rivers. These areas either underlie or fringe the locations in the maps of satellite-derived TSM concentration that show limited or no annual cycle, suggesting that the satellite may not be able to resolve changes in TSM in these areas.

Furthermore, the distinguishing of the seabed at low tide from TSM-rich water at high tide is difficult over the shallow regions of Minas Basin.

Sediment concentrations may be too high for accurate estimation by the MERIS algorithm. Based on the Crewe's *in situ* measurements (Crewe, 2004), the surficial mean suspended sediment concentration is approximately 50 g/m^3 during the whole summer at the head of Salmon River Estuary. Concentrations of this magnitude are at the upper limit that can be resolved by MERIS (Shen et al., 2010a). Concentrations of more than 150 g/m^3 have been observed at the head of Cobequid Bay in the eastern portions of the Minas Basin (Parker et al., 2007). Interestingly, the mean of satellite TSM concentration at the head of Cobequid Bay was below 10 g/m^3 during the summer (Fig. 3). Similarly, recorded surficial TSM concentration greater than 100 g/m^3 has been observed near the mouth of the Cornwallis River in the Southern Bight, but such large concentrations do not exist in this area according to the satellite-derived data (Parker et al., 2007). It is difficult to compare *in situ* samples and remotely sensed concentrations directly (Eleveld et al., 2008) because samples must be collected at the same time as a satellite overflight and the satellite estimate is an average over a large spatial area. Nonetheless, observed differences in this study suggest that MERIS consistently underestimates TSM concentration in environments where sediment concentrations are large. Such underestimation may explain why the model predicts greater seasonal variability over tidal flats than the satellite TSM show. Unfortunately, there were no data to evaluate the MERIS TSM data in winter at Cobequid Bay.

It should be noted finally that MERIS might work reasonably well in Minas Basin because inorganic sediment concentrations are so high. The suspended inorganic matter reflects light to a much greater extent than other substances.

4.3.2. Accuracy of Delft3D TSM concentration

The model predictions may be inaccurate in shallow areas because initial conditions were formulated improperly, some physical processes were not considered, or bathymetry was inaccurate.

In Minas Basin, the model shows that the fine suspended sediment concentration and the distribution of mud on the surface are controlled by a combination of the sediment parameters and the physical processes that cause re-suspension and transport. The distribution of sediment on the bed for the initial condition is highly simplified in that it treats the bottom either as mud-covered or bare. The effect of sand re-suspension over the shallow flats is neglected. Consideration of sand could enhance rather than reduce seasonal differences in the model output due to increased re-suspension of sand by waves during more energetic winter months. Delft3D may not predict TSM concentration over shallow areas because in this study it did not include some processes that re-suspend sediment. Perhaps most importantly, the model did not include waves, which are important for re-suspending sediment in shallow water. In the intertidal zone of Minas Basin, wave activity on the tidal flats is very important in creating turbid conditions that characterize the Cobequid Bay and Windsor Bay (Parker et al., 2007). Inclusion of waves would enhance rather than reduce seasonal differences in modelled TSM concentration. Another question is whether the model bathymetry of Minas Basin is accurate. The suspended sediment sources are the shallow areas of Cobequid Bay and Windsor Bay where bathymetry is dynamic and poorly resolved. Inaccurate bathymetry can degrade model predictions, but it is unlikely any inaccuracies would introduce seasonal bias into model results.

4.3.3. Accuracy of comparison

The differences between model and satellite TSM concentration patterns might be caused by the time averaging technique. As mentioned before, the seasonal mean of the satellite TSM concentrations were derived from the time averaging of two months of satellite data, but the mean of the model TSM was obtained by averaging of two days model output. MERIS satellite overpasses the study area daily, and the model simulated the TSM hourly. Although the time averaging technique may induce magnitude differences, it should not influence the TSM concentration distribution or variation in the entire Basin or produce an artificial seasonal signal over shallow areas. Additionally, the timing within the tidal cycle also causes a bias in the MERIS results.

The differences between model and satellite TSM concentration pattern might be caused by the portion of the water column measured. The vertical resolution of Delft3D model is variable in Minas Basin, so the layer thickness at the surface varied between locations. The surface layer thickness varied from 1 to 12 m. However, the portion of the water column MERIS measured is based on the path of photons through the water column. The geometrical thickness of the water layer from which 90% of the remotely sensed ocean colour signal comes can be approximated by the vertical attenuation coefficient for downward irradiance, so the geometrical thickness of water column is determined according to the concentrations and inherent optical properties of water substances (MERIS product handbook, 2006). The satellite-based TSM in Minas Basin derives from a thin surficial layer of the water column, and it does not include deeper layers that contribute to the model estimate of surficial TSM concentration. In short, the optical depth of the satellite is shallower than the model's surface layer.

The observed annual cycle of TSM in the centre of Minas Basin is likely real, but the lack of an annual cycle in satellite-derived TSM over shallow areas is questionable. Model simplifications and inaccuracies are unlikely to produce a spurious seasonal difference between summer and winter simulations. In fact, omitted processes like waves and sand transport are likely to enhance rather than limit the seasonal differences predicted by the model.

5. Conclusions

Ocean colour data from the satellite-based MERIS sensor were used to determine the spatial distribution of suspended sediment in the macro-tidal coastal embayment of Minas Basin. The mean values of TSM concentration over 1 km^2 pixel boxes derived from MERIS data indicate an annual change in most areas of Minas Basin. Higher TSM concentrations were observed in late-winter (February and March), and lower TSM concentrations characterized late-summer (July and August). Averaged over the entire Basin, the TSM magnitude generally varied from 15 to 45 g/m^3 in winter and was below 20 g/m^3 in summer. Temporal autocorrelation analysis was carried out with TSM time series throughout the Basin. The strength of annual signal varied throughout the Basin, with the largest variation occurring in the central part of Minas Basin, and the smallest variation occurring in Cobequid Bay, near Windsor Bay and along the boundaries of the Basin.

Satellite-derived TSM concentrations were compared with TSM derived from the three-dimensional Delft3D model. The modelling approach was to vary sediment parameters on the tidal flats of the Basin while maintaining the same hydrodynamic conditions. The motivation for this approach was to examine the extent to which changes in biologically mediated erodibility of shallow water sediments could account for the observed seasonal changes in TSM. Quantitative comparisons between model and satellite-derived TSM during the summer and winter showed similar magnitudes and spatial distributions could be achieved by reducing the erosion rate of sediments on the shallow seabed by an order of magnitude between winter and summer. Agreement was not good, however, over the shallow regions fringing the central Basin. The Delft3D model typically over-predicted TSM concentration relative to satellite-derived estimates in the shallow areas in winter and under-predicted TSM in shallow areas in summer. The source of the discrepancies in shallow water may be due to model assumptions or initial conditions, but it more likely arises from inaccurate retrieval of TSM concentration by the satellite in these regions. Arguably the most important next step is quantifying how the biological activity on the bottom of the seabed affects on the dynamics of cohesive sediment on large spatial and temporal scales in the Minas Basin. In the future, model parameterization of erosion rate should be based on *in situ* measurements of biofilm properties and erosion rates observed throughout the seasonal cycle in macrotidal environments like Minas Basin.

Acknowledgments

The authors wish to thank Carla Caverhill and Cathy Porter from Bedford Institute of Oceanography for kindly providing MERIS satellite data, and also Gary Bugden, Tim Milligan, Ed Horne, and Brent Law for providing relevant filed data from Minas Basin. This research was funded by the Offshore Energy Environmental Research Association (OEER), Offshore Energy Research Association of Nova Scotia (OERA) through grant 300-170-09-13, Natural Sciences and Engineering Research Council of Canada (NSERC) and Dalhousie University.

Appendix A. Supplementary data

Supplementary data related to this article can be found at http://dx.doi.org/10.1016/j.ecss.2014.10.005.

References

Amos, C.L., Alfoldi, T.T., 1979. The determination of suspended sediment concentration in a macrotidal system using Landsat data. J. Sediment. Petrol. 49 (1), 0159–0173.
Amos, C.L., Long, B.F.N., 1980. In press: The sedimentary character of the MinasBasin System, Bay of Fundy; in The Coastline of Canada. In: McCann, S.B. (Ed.), Geological Survey of Canada, pp. 123–152.
Amos, C.L., Mosher, D.C., 1985. Erosion and deposition of fine-grained sediments from the Bay of Fundy. Sedimentology 32 (6), 815–832.
Amos, C.L., Joice, G.H.E., Oceanography, B. I. o, 1977. The Sediment Budget of the Minas Basin, Bay of Fundy, N.S. Bedford Institute of Oceanography.
Amos, C.L., Daborn, G.R., Christian, H.A., 1992. In situ erosion measurements on fine-grained sediments from the Bay of Fundy. Marine Geology 108, 175–196.
ATBD Chapter 2.12, The Algorithm Theoretical Basis Documents of the MERIS Level 2, GKSS Research Centre, EAS
Babin, M., Morel, A., Fournier-Sicre, V., Fell, F., Stramski, D., 2003. Light scattering properties of marine particles in coastal and open ocean waters as related to the particle mass concentration. Limnol. Oceanogr. 48 (2), 843–859.
Berry, J.K., 1999. Use statistics to compare map surfaces. Beyond Mapp. column, GEO World 23–24. October issue.
Bianchi, T.S., 2007. Biogeochemistry of Estuaries. Oxford University Press, p. 720.
Borsje, Bas W., de Vries, Mindert B., Hulscher Suzanne, J.M.H., de Boer, Gerben J., 2008. Modeling large-scale cohesive sediment transport affected by small-scale biological activity. Estuar. Coast. Shelf Sci. 78 (3), 468–480.
Bourg, L., Delwart, S., Huot, J.P., Rast, A., 2002. Calibration and early results of MERIS on ENVISAT. In: Geoscience and Remote Sensing Symposium and 24th Canadian Symposium on Remote Sensing. Proceedings: Remote Sensing: Integrating Our View of the Planet, vol. I-Vi, pp. 599–601.
Bowers, D.G., Braithwaite, K.M., Nimmo-Smith, W.A.M., Graham, G.W., 2009. Light scattering by particles suspended in the sea: the role of particle size and density. Cont. Shelf Res. 29 (14), 1748–1755.
Bugden, G., Milligan, T., Law, B., 2007. The Distribution of Suspended Particulate Matter in Northumberland Strait, in Atlantic Canada Coastal and Estuarine Science Society Annual Meeting, Cape Breton University.
Carrière-Garwood, J., 2013. Seasonal Variation and Biological Effects on Mudflat Erodibility in the Minas Basin, Bay of Fundy. Master's thesis. Dalhousie University.
Crewe, B., 2004. Characterization of Sediment in the Salmon River Estuary. MSc. thesis. Dalhousie University, unpublished.
Dalrymple, R.W., Knight, R.J., Zaitlin, B.A., Middleton, G.V., 1990. Dynamics and facies model of a macrotidal sand-bar complex, Coqequid Bay salmon river estuary (Bay of Fundy). Sedimentology 37 (4), 577–612.
Diggle, P., 1990. Time Series: a Biostatistical Introduction. Clarendon Press.
Doerffer, R., Schiller, H., 2007. The MERIS case 2 water algorithm. Int. J. Remote Sens. 28 (3–4), 517–535.
Eleveld, M.A., Pasterkamp, R., van der Woerd, H.J., Pietrzak, J.D., 2008. Remotely sensed seasonality in the spatial distribution of sea-surface suspended particulate matter in the southern North Sea. Estuar. Coast. Shelf Sci. 80 (1), 103–113.
ESA website: https://earth.esa.int/web/guest/data-access.
European Space Agency, 2006. MERIS Product Handbook from. http://earth.esa.int/pub/ESA_DOC/ENVISAT/MERIS/meris.ProductHandbook.2_1.pdf.
Fader, G.B., King, L.H., MacLean, B., Service, C.H., 1977. Surficial Geology of the Eastern Gulf of Maine and Bay of Fundy. Fisheries and Environment Canada, Fisheries and Marine Service.
Greenberg, D.A., Amos, C.L., 1983. Suspended sediment transport and deposition modeling in the Bay of Fundy, Nova Scotia – a region of potential tidal power development. Can. J. Fish. Aquatic Sci. 40, 20–34.
Hayes, M.O., 1975. Morphology of sand accumulation in estuaries: an introduction to the symposium. In: Cronin, L.E. (Ed.), Estuarine Research, vol. II. Academic Press, New York, pp. 3–22.
Hill, P.S., Milligan, T.G., Geyer, W.R., 2000. Controls on effective settling velocity of suspended sediment in the Eel River flood plume. Cont. Shelf Res. 20 (16), 2095–2111.
Houwing, E.J., 1999. Determination of the critical erosion threshold of cohesive sediments on intertidal mudflats along the Dutch Wadden Sea coast. Estuar. Coast. Shelf Sci. 49, 545–555.
Hu, K., Ding, P., Wang, Z., Yang, S., 2009. A 2D/3D hydrodynamic and sediment transport model for the Yangtze Estuary, China. J. Mar. Syst. 77, 114–136.
Lesser, G.R., Roelvink, J.A., van Kester, J., Stelling, G.S., 2004. Development and validation of a three-dimensional morphological model. Coast. Eng. 51 (8–9), 883–915.
Mikkelsen, O.A., Milligan, T.G., Hill, P.S., Moffatt, D., 2004. INSSECT - an instrumented platform for investigating floc properties close to the seabed. Limnol. Oceanogr. 2, 226–236.
Mitchell, S.B., Uncles, R.J., 2013. Estuarine sediments in macrotidal estuaries: future research requirements and management challenges. Ocean Coast. Manag. 79, 97–100.
Morris, R.K.A., 2013. Geomorphological analogues for large estuarine engineering projects: a case study of barrages, causeways and tidal energy projects. Ocean Coast. Manag. 79, 52–61.
Mulligan, R., Smith, P., Hill, P.S., Tao, J., van Proosdij, D., 2013. Effect of Tidal Power Generation on Hydrodynamics and Sediment Processes in the Upper Bay of Fundy. Proc. Can. Soc, Civil. Eng., Montreal, QC.
Parker, M., Westhead, M., Doherty, P., Naug, J., 2007. Canadian manuscript report of fisheries and aquatic sciences 2789-2007 Ecosystem overview and assessment report for the Bras D'Or Lakes, Nova Scotia - Introduction. Can. Manuscr. Rep. Fish. Aquatic Sci. 2789, 1–192, 194-211,212-220,222,XV,XVI,XVII.
Shen, F., Salama, M.S., Zhou, Y.X., Li, J.F., Su, Z., Kuang, D.B., 2010a. Remote-sensing reflectance characteristics of highly turbid estuarine waters - a comparative experiment of the Yangtze River and the Yellow River. Int. J. Remote Sens. 31 (10), 2639–2654.
Shen, F., Verhoef, W., Zhou, Y., Salama, M.S., Liu, X., 2010b. Satellite estimates of wide-range suspended sediment concentrations in Changjiang (Yangtze) estuary using MERIS data. Estuaries Coasts 33 (6), 1420–1429.
Stea, R., 2003. A Virtual Fieldtrip of the Landscapes of Nova Scotia. Nova Scotia Department of Natural Resources, NS.
Sutherland, J., Walstra, D.J.R., Chesher, T.J., van Rijn, L.C., Southgate, H.N., 2004. Evaluation of coastal area modelling systems at an estuary mouth. Coast. Eng. 51 (2), 119–142.
Thomas, M.L.H., 1976. Intertidal Resources of the Bay of Fundy, Fundy Tidal Power and the Environment. Acadia University, Wolfville, NS.
van Proosdij, D., Milligan, T., Bugden, G., Butler, K., 2009. A tale of two macro tidal estuaries: differential morphodynamic response of the intertidal zone to causeway construction. J. Coast. Res. 772–776.
Winterwerp, J.C., 2002. On the flocculation and settling velocity of estuarine mud. Cont. Shelf Res. 22 (9), 1339–1360.
WL|Delft Hydraulics, 2006. User Manual Delft3D-FLOW. WL|Delft Hydraulics, Delft.
Wu, Y., Chaffey, J., Greenberg, D.A., Colbo, K., Smith, P.C., 2011. Tidally-induced sediment transport patterns in the upper Bay of Fundy: a numerical study. Cont. Shelf Res. 31 (19), 2041–2053.